IMPEDANCE BUDGET FOR EIC BEAM ACCUMULATOR RING

A. Khan*, V. Smaluk, R. Todd, M. Seegitz
NSLS-II, BNL, Upton, NY, USA

Abstract

The Beam Accumulator Ring (BAR) in the Electron–Ion Collider (EIC) injector chain is designed to accumulate charge from multiple linac pulses to produce a high-intensity polarized electron beam for injection into the Electron Storage Ring. At the design single-bunch charge, beam–impedance effects become an important factor for beam stability and component heating. In this work, we develop a longitudinal impedance model of the BAR, combining electromagnetic simulations of the main vacuum components with analytical estimates of the resistive-wall contribution. The total impedance is evaluated by combining all contributions, and key parameters relevant for beam dynamics are extracted. The results provide a consistent basis for assessing collective effects and guiding further optimization of the vacuum chamber design.

INTRODUCTION

The Electron-Ion Collider (EIC) project is under development at Brookhaven National Laboratory to explore the fundamental structure of matter [1]. The Beam Accumulator Ring (BAR) is part of the EIC injector chain [2]. Located between the 750 MeV linac and the 5–18 GeV Rapid Cycling Synchrotron, BAR accumulates charge from multiple linac pulses to provide the high-intensity polarized electron beam required for downstream acceleration and injection into the Electron Storage Ring (ESR).

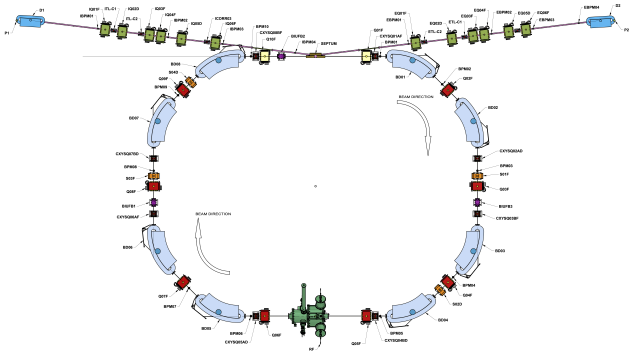

Figure 1: Layout of the Beam Accumulator Ring with injection and extraction transfer lines.

Figure 1 shows the layout of the Beam Accumulator Ring (BAR), including its lattice components such as dipoles, quadrupoles, sextupoles, RF cavities, injection, and extraction systems. The beam is injected from the 750 MeV linac into BAR at a repetition rate of 30 Hz with an initial charge of about 1.1 nC per bunch. Once the single-bunch charge reaches 28 nC (with design margin up to 32 nC), the beam is extracted and transferred to the Rapid Cycling Synchrotron for further acceleration before injection into the ESR.

Achieving this high single-bunch charge presents a major challenge for the BAR design. The interaction of such an intense beam with the vacuum chamber impedance can drive instabilities and cause local overheating of components if the impedance is not carefully controlled. A realistic ring-wide impedance budget is therefore essential for evaluating performance and stability limits.

The present BAR design is based on the NSLS VUV ring lattice and vacuum chamber concept. We have modified and optimized it to satisfy the specific requirements of the EIC injector, including high bunch charge, polarization preservation, and interfaces with the injection/extraction transport lines.

In the original NSLS VUV ring, the bellows contributed the largest share of the geometric impedance [3]. For the BAR design, RF-shielded bellows have been implemented to mitigate this effect. Figure 2 shows the geometries of the unshielded and RF-shielded bellows used in the simulations.

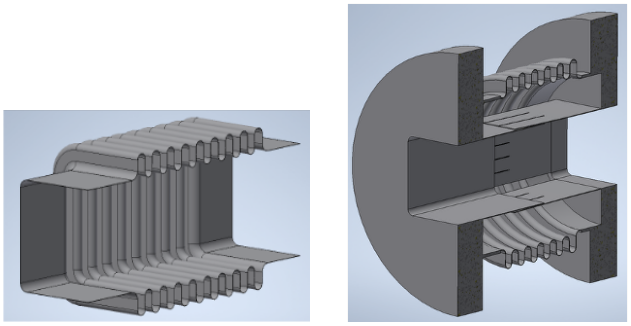

Figure 2: Schematic views of the bellows geometry used in the impedance simulations: (left) unshielded bellows and (right) RF-shielded bellows design with cross-section of 80 mm × 40 mm.

The longitudinal impedance of the bellows was evaluated for both configurations. As shown in Fig. 3, the unshielded bellows exhibit a significantly larger impedance over a broad frequency range, while the RF-shielded design strongly suppresses both the real and imaginary parts of the impedance.

This reduction is also reflected in the loss factor k_{loss}, which quantifies the energy loss per unit charge due to wake-fields. For the present bunch length $\sigma_s = 61.5$ mm, the loss factor decreases from 0.31 mV/pC for the unshielded case to 7×10^{-4} mV/pC with RF shielding, corresponding to a reduction by more than two orders of magnitude. This demonstrates that RF-shielded bellows are essential for achieving a low overall impedance budget in the BAR, as reflected in the total impedance model discussed below.

* akhan1@bnl.gov

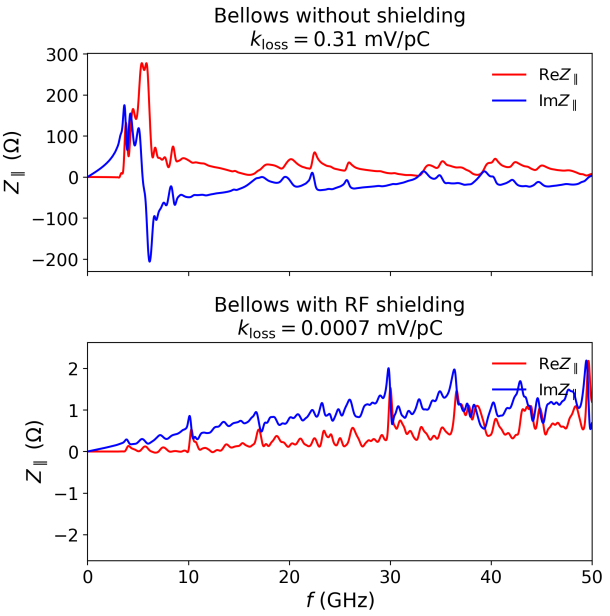

Figure 3: Longitudinal impedance of the bellows without RF shielding (top) and with RF shielding (bottom). Note the different vertical scales.

IMPEDANCE MODEL

The BAR impedance model includes both the resistive-wall impedance of the vacuum chamber and the geometric impedance of the main vacuum components. The geometric impedance was computed with the 3D electromagnetic solver GdfidL [4], while the resistive-wall contribution was evaluated analytically for the nominal rectangular aluminum chamber with cross section 80 mm × 40 mm [5]. In the resistive-wall calculation, the chamber material was assumed to be aluminum with resistivity $\rho_{Al} = 2.8 \times 10^{-8}\,\Omega\,\mathrm{m}$.

In the wakefield simulations, a short Gaussian bunch was used to resolve the high-frequency part of the impedance spectrum and to capture the effect of small geometric features. The bunch length was chosen to be shorter than the relevant feature sizes of the vacuum components, which reduces numerical smearing and provides a more reliable estimate of the broadband geometric impedance [6].

The main vacuum components included in the impedance budget are listed below. Their contributions are combined to obtain the total BAR impedance model.

- Bellows with RF shield (2 per dipole): 16
- Flanges with RF contact spring: 44 (2 per bellows × 16 + 2 per kicker × 3 + 2 for the septum + 4 for the RF cavity)
- Button pickup assemblies: 11
- Gate valves (injection and RF straight sections): 4
- Pumping ports: 16
- Ceramic kickers with tapered transitions: 3
- Clearing electrodes: 16

Figure 4 shows the longitudinal impedance of the main BAR vacuum components used in the present geometric impedance model. The real and imaginary parts of $Z_{\parallel}$ are plotted for the bellows, BPM, kicker tapers, clearing electrodes, flanges, gate valves, and pumping ports. The flange and BPM contributions are the dominant localized sources over a broad part of the frequency range, while the other components remain comparatively smaller.

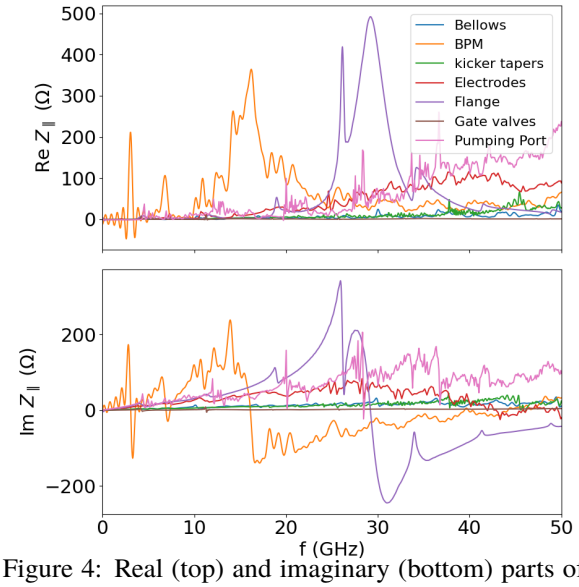

Figure 4: Real (top) and imaginary (bottom) parts of the longitudinal impedance of the individual BAR vacuum components included in the geometric impedance model.

Kicker Ceramic Chambers

The BAR injection and extraction system uses fast kickers that generate pulses shorter than the revolution period, allowing single-turn beam deflection. Each kicker is 30 cm long, and the ceramic chamber has the same cross section as the nominal vacuum chamber, 80×40 mm^2. The inner surface of the ceramic chamber is coated with a 3 µm titanium layer to provide a conducting path for the high-frequency beam image current while remaining sufficiently transparent to the kicker pulse field.

Using the measured titanium resistivity, $\rho = 3.85 \times 10^{-6}\,\Omega\cdot\mathrm{m}$, and Eq. 1 in Ref. [7], we estimated the longitudinal impedance of the Ti-coated ceramic chamber, assuming a ceramic wall thickness of 6 mm. The result is shown in Fig. 5. In addition, the contribution from tapered transitions at the kicker ends was computed and included in the geometric impedance budget.

Total Impedance

The total longitudinal impedance of the BAR is obtained by summing the contributions from all geometric components together with the resistive-wall impedance. Figure 6 shows the resulting real and imaginary parts of the total

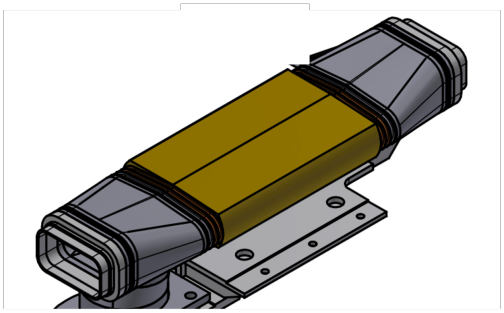

(a) Schematic of the Ti-coated ceramic kicker chamber.

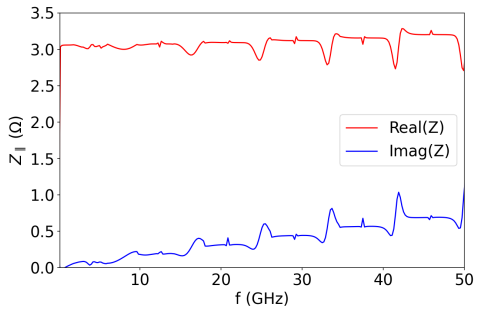

(b) Longitudinal impedance of the Ti-coated ceramic chamber for a coating thickness of 3 µm.

Figure 5: Ceramic kicker chamber geometry and corresponding longitudinal impedance.

impedance. The broadband behavior is dominated by localized components such as flanges and BPMs, while the resistive-wall contribution mainly affects the low-frequency region.

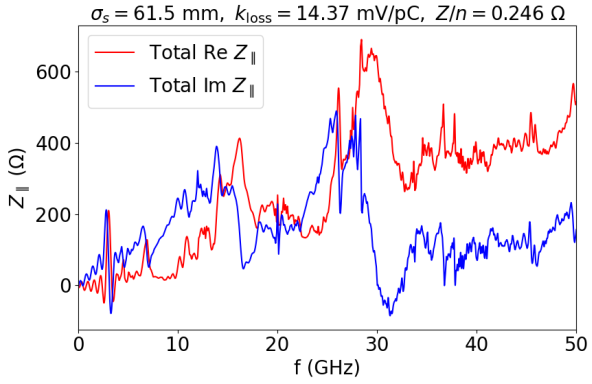

Figure 6: Real (red) and imaginary (blue) parts of the total longitudinal impedance $Z_\parallel$ of the BAR, including both geometric and resistive-wall contributions.

The resulting impedance does not show strong narrowband features, indicating effective suppression of resonant contributions. The smooth behavior at high frequencies reflects the use of RF shielding and tapered transitions in minimizing geometric discontinuities. The normalized impedance Z/n extracted from the model provides a useful figure of merit for evaluating single-bunch collective effects, in particular the threshold for microwave instability.

CONCLUSION

In this work, we developed a comprehensive longitudinal impedance model for the EIC Beam Accumulator Ring, combining 3D electromagnetic simulations of the main vacuum components with analytical resistive-wall contributions. The results show that localized elements such as flanges and BPMs dominate the broadband geometric impedance, while the resistive-wall contribution is significant at low frequencies. The total impedance, along with the extracted loss factor and normalized impedance, provides a consistent basis for evaluating beam stability and beam-induced heating. These results are an important input for further optimization of the BAR design and for assessing collective effects at the design bunch charge.

REFERENCES

[1] C. Montag *et al.*, "The EIC accelerator: design highlights and project status", in *Proc. IPAC'24*, Nashville, TN, USA, May 2024, pp. 214–217. doi:10.18429/JACoW-IPAC2024-MOPC67

[2] A. Khan and V. Smaluk, "Analytical estimates of beam intensity limitations in the EIC beam accumulator ring", Brookhaven National Laboratory, Upton, NY, USA, Rep. BNL-229164-2025-TECH, NSLSII-ASD-TN-436, Nov. 2025. doi:10.2172/3005213

[3] J. Galayda *et al.*, "Experience with a high-brightness storage ring: the NSLS 750 MeV VUV ring", *Nucl. Instrum. Methods Phys. Res. A*, vol. 239, no. 1, pp. 106–109, 1985.

[4] W. Bruns, "GdfidL", http://www.gdfidl.de/,

[5] R. L. Gluckstern, J. van Zeijts, and B. Zotter, "Coupling impedance of beam pipes of general cross section", *Physical Review E*, vol. 47, no. 1, pp. 656–663, 1993. doi:10.1103/PhysRevE.47.656

[6] A. Khan and V. Smaluk, "Convergence study of wakefield simulations with GdfidL and ECHO3D", *Nucl. Instrum. Methods Phys. Res. A*, vol. 1082, p. 171073, 2025. doi:10.1016/j.nima.2025.171073

[7] A. Khan *et al.*, "Simulation and measurement of beam-induced heating of ceramic vacuum chambers", *Physical Review Accelerators and Beams*, vol. 27, no. 8, p. 084501, 2024. doi:10.1103/PhysRevAccelBeams.27.084501